PLOS PATHOGENS

RESEARCH ARTICLE

Novel regulators of PrP^C biosynthesis revealed by genome-wide RNA interference

Daniel Heinzer[1☯], Merve Avar[1☯], Daniel Patrick Pease[1‡], Ashutosh Dhingra[2‡], Jiang-An Yin[1], Elke Schaper[1], Berre Doğançay[1], Marc Emmenegger[1], Anna Spinelli[1], Kevin Maggi[1], Andra Chincisan[1], Simon Mead[3], Simone Hornemann[1], Peter Heutink[2], Adriano Aguzzi[1]*

1 Institute of Neuropathology, University of Zurich, Zurich, Switzerland, **2** German Center for Neurodegenerative Diseases (DZNE), Tübingen, Germany, **3** MRC Prion Unit at UCL, Institute of Prion Diseases, London, United Kingdom

☯ These authors contributed equally to this work.
‡ DPP and AD are both second authors
* adriano.aguzzi@usz.ch

Citation: Heinzer D, Avar M, Pease DP, Dhingra A, Yin J-A, Schaper E, et al. (2021) Novel regulators of PrP^C biosynthesis revealed by genome-wide RNA interference. PLoS Pathog 17(10): e1010013. https://doi.org/10.1371/journal.ppat.1010013

Editor: Jason C. Bartz, Creighton University, UNITED STATES

Received: September 28, 2021

Accepted: October 7, 2021

Published: October 27, 2021

Data Availability Statement: All relevant data are within the manuscript and its Supporting Information files, and the Data analysis pipeline can be found online at https://github.com/elkeschaper/hts.

Funding: AA is the recipient of an Advanced Grant of the European Research Council (670958) and grants from the Swiss National Research Foundation (179040), the Nomis Foundation, the Swiss Personalized Health Network (SPHN, 2017DRI17) and a donation from the Estate of Dr. Hans Salvisberg. DH is the recipient of a ZNZ

Abstract

The cellular prion protein PrP^C is necessary for prion replication, and its reduction greatly increases life expectancy in animal models of prion infection. Hence the factors controlling the levels of PrP^C may represent therapeutic targets against human prion diseases. Here we performed an arrayed whole-transcriptome RNA interference screen to identify modulators of PrP^C expression. We cultured human U251-MG glioblastoma cells in the presence of 64'752 unique siRNAs targeting 21'584 annotated human genes, and measured PrP^C using a one-pot fluorescence-resonance energy transfer immunoassay in 51'128 individual microplate wells. This screen yielded 743 candidate regulators of PrP^C. When downregulated, 563 of these candidates reduced and 180 enhanced PrP^C expression. Recursive candidate attrition through multiple secondary screens yielded 54 novel regulators of PrP^C, 9 of which were confirmed by CRISPR interference as robust regulators of PrP^C biosynthesis and degradation. The phenotypes of 6 of the 9 candidates were inverted in response to transcriptional activation using CRISPRa. The RNA-binding post-transcriptional repressor Pumilio-1 was identified as a potent limiter of PrP^C expression through the degradation of *PRNP* mRNA. Because of its hypothesis-free design, this comprehensive genetic-perturbation screen delivers an unbiased landscape of the genes regulating PrP^C levels in cells, most of which were unanticipated, and some of which may be amenable to pharmacological targeting in the context of antiprion therapies.

Author summary

The cellular prion protein (PrP^C) acts as both, the substrate for prion formation and mediator of prion toxicity during the progression of all prion diseases. Suppressing the levels of PrP^C is a viable therapeutic strategy as *PRNP* null animals are resistant to prion disease and the knockout of *PRNP* is not associated with any severe phenotypes. Motivated by the

Forschungskredit Candoc grant (FK-18-031). The funders had no role in study design, data collection and analysis, decision to publish, or preparation of the manuscript.

Competing interests: The authors have declared that no competing interests exist.

scarcity of knowledge regarding the molecular regulators of PrP^C biosynthesis and degradation, which might serve as valuable targets to control its expression, here, we present a cell-based genome wide RNAi screen in arrayed format. The screening effort led to the identification of 54 regulators, nine of which were confirmed by an independent CRISPR-based method. Among the final nine targets, we identified PUM1 as a regulator of *PRNP* mRNA by acting on the 3'UTR promoting its degradation. The newly identified factors involved in the life cycle of PrP^C provided by our study may also represent themselves as therapeutic targets for the intervention of prion diseases.

Introduction

A feature common to all prion diseases is the conversion of the cellular prion protein (PrP^C) into a misfolded, disease-causing isoform called PrP^{Sc} [1]. PrP^C is an agonist of the adhesion G protein-coupled receptor Adgrg6 in the peripheral nervous system, but its role in the central nervous system (CNS) has remained unclear [2,3]. In prion disease, PrP^C is not only necessary for the generation of PrP^{Sc} but is also involved in mediating neurotoxicity [4]. Many lines of evidence indicate that PrP^C is rate-limiting for the progression of prion diseases, and hemizygous $Prnp^{+/o}$ mice expressing approximately 60% of wildtype PrP^C levels enjoy a vastly extended life expectancy after prion inoculation [5]. Therefore, it was proposed that quenching the availability of PrP^C may represent a feasible therapeutic strategy against prion diseases [6].

A number of candidate compounds binding to or lowering PrP^C levels have been reported [7,8]. However, small molecules often display pleiotropic actions and off-target effects, and compounds that lack a well-defined target do not allow drawing far-reaching conclusions about the biosynthesis of PrP^C. Therefore, only few modulators of PrP^C biosynthesis, including the transcription factors sXBP1 and SP1 and the direct interactor, LRP1, were identified thus far [9–17].

Here we have assessed the expression of PrP^C in the human CNS-derived glioblastoma cell line, U251-MG, after downregulation of each protein-coding gene by arrayed RNA interference (RNAi). The screen yielded 54 novel regulators of PrP^C. Nine of those could be validated through an inhibitory CRISPR assay (CRISPRi), and six showed inverted-polarity PrP^C regulation by activating CRISPR (CRISPRa). This unbiased approach enabled the discovery of unanticipated molecular players regulating PrP^C expression levels. The cell-based screening and validation methodologies described here can be easily adapted to identify regulators of the expression of any other protein of interest.

Results

Primary screening for regulators of PrP^C expression

To gain insight into proteins that affect PrP^C expression, we performed a high-throughput whole genome RNAi screen in a human glioblastoma derived cell line, U251-MG. We chose this cell line because of its euploid karyotype and its relatively high PrP^C expression level, ranking 15th of 69 cell lines in a protein atlas [18,19]. We did not determine the M/V genotype of the cells as there is no evidence that it would influence PrP^C expression. U251-MG cells were successfully utilized in a high-throughput screen for miRNA regulators of PrP^C expression [20]. We used a commercially available siRNA library consisting of 64'752 unique siRNAs targeting 21'584 annotated human genes. For the primary screening round, three distinct equimolar siRNAs targeting the same transcript were pooled into 21'584 individual wells of 62

plates (1.67 μM per siRNA) to a final concentration of 5 μM. This library was denoted as "pooled library". Subsequently, siRNAs were reformatted into final assay destination plates to a final concentration of 5 nM using an ECHO555 acoustic dispenser.

We developed a specialized plate layout with the goal of maximizing the randomization of replicas and therefore minimizing the impact of systematic errors. Each assay was run in duplicates dispensed on two individual plates and in two distinct plate locations. We used a cell-death inducing siRNA (20 nM) to control for reduction in viability (n = 22 per plate) as well as pool of non-targeting (NT) siRNAs (n = 44 per plate, 5 nM)) and a pool of *PRNP*-targeting siRNAs (n = 22 per plate, 5 nM). Controls were distributed in a checkerboard pattern across the plate with the aim of identifying any systematic errors deriving from gradients that may arise in the plates during protracted cell culture (Fig 1A). Assay plates containing the siRNAs were thawed, and U251-MG cells were seeded following reverse transfection with Lipofectamine.

After three days of culture, cells were lysed and PrP^C levels was measured using a solution-based immunoassay. Two antibodies directed against non-overlapping epitopes of PrP^C, POM2 coupled to Europium (POM2-EU) as donor and POM1 coupled to allophycocyanin (POM1-APC) as acceptor, were added to the lysates. Binding of the antibodies to PrP^C brings the europium and the allophycocyanin into close proximity, allowing for time-resolved fluorescence resonance energy transfer (TR-FRET) and emission of longer-wavelength light whose intensity is proportional to the concentration of PrP^C [20–23]. For quality control, we first inspected heat maps plotted for raw TR-FRET values per well after correction for spectral overlapping [21]. We then calculated the standardized mean difference (SSMD) and Z' factor [24,25] reporting the separation of positive (*PRNP* targeting siRNAs) and negative (NT siRNAs) controls.

We measured 166 plates of 384 wells, totaling 63'744 measurements. The outermost wells did not contain any samples and were excluded from Z' factor and SSMD calculations due their proneness for evaporation (Figs 1C and 1D and S1A). We considered that inhomogeneities of temperature, humidity or CO_2 concentration during tissue culturing might create artifactual signal gradients which could impair the interpretation of the results. However, no such artifacts were observed across the whole-genome dataset. Z' factors, which report the discriminatory power between positive and negative control, were >0.5 and 0–0.5 for 157 and 9 plates respectively. These values indicate that the screen was robust and allowed for reliable hit calling [24]. Inter-plate variability was assessed by calculating the Pearson correlation coefficient between duplicates, and yielded a value of 0.56, indicating that the screen data was sufficiently robust to select candidate genes (Fig 1E). We used strictly standardized mean differences (SSMD) to assess the effect of each target on PrP^C expression [25]. Targets with an effect size <-4 or >4 on PrP^C expression were considered candidates for a secondary screen. We selected this threshold based on the weakest cumulative SSMD for controls on all plates (S1A Fig), found to be -5, to be inclusive of all candidates of interest. As discordant duplicates occurred rarely (Fig 1E), they were also included as candidate genes if reaching the threshold of $p > 10^{-15}$ (Student's t-test) which is not sensitive to replica discrepancies.

In summary, 743 out of 21'584 tested genes were selected as candidates to be assessed in a secondary screen (SSMD < -4 or > 4 and/or $p > 10^{-15}$; Sheets A and B in S1 Table). When suppressed by siRNA, 563 of these reduced and 180 genes increased PrP^C levels (Fig 1F). We shall henceforth refer to such genes as "stabilizers" and "limiters" of PrP^C expression, respectively.

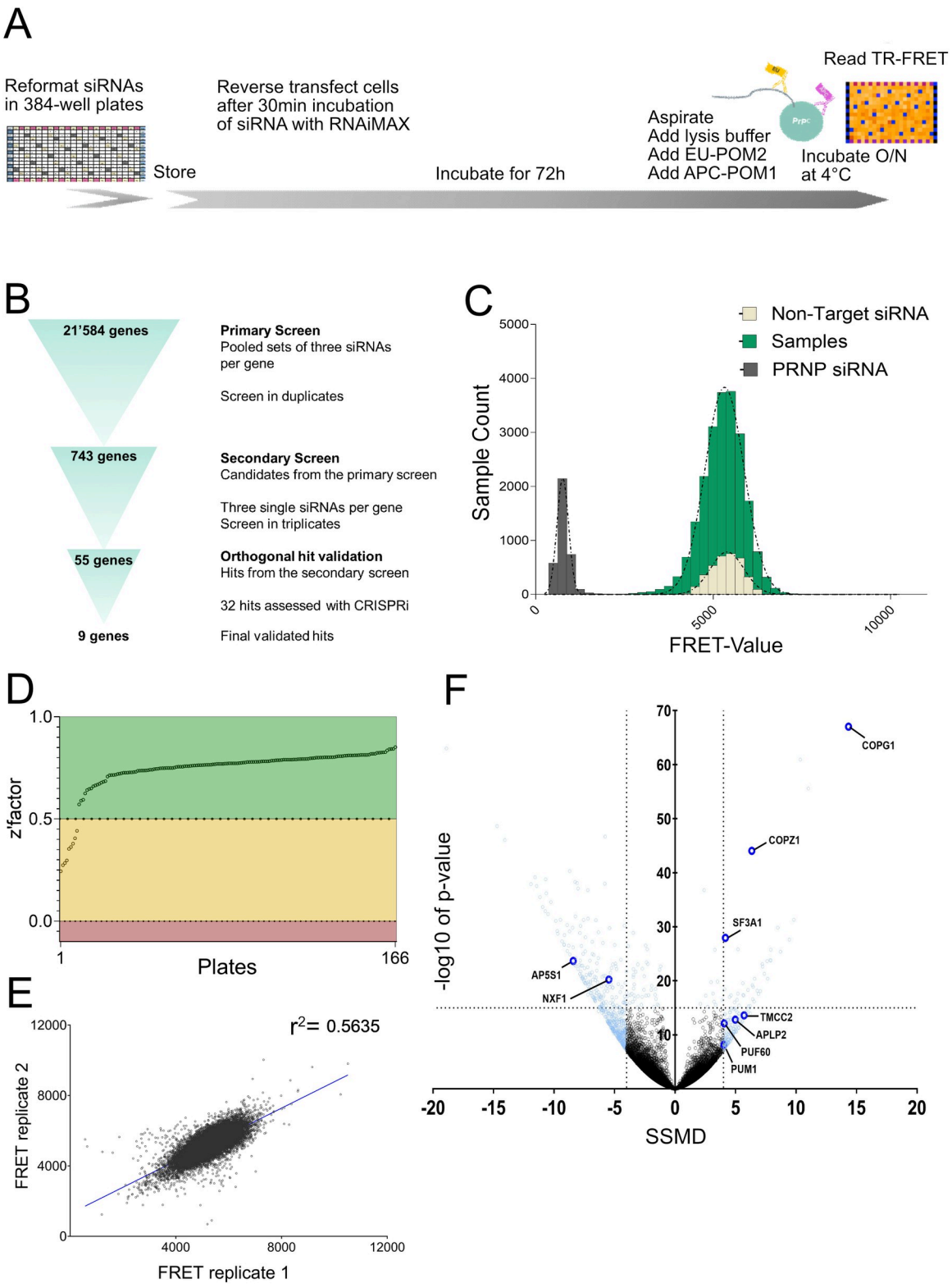

Fig 1. Workflow of the siRNA screen and primary screening round in U251-MG glioblastoma cell line. (A) Depiction of the screening workflow. (B) Hit selection process. (C) Distribution of populations of positive controls (*PRNP* targeting siRNAs), negative controls (non-targeting siRNAs) and samples (contents of whole genome siRNA libraries) across FRET values. The x-axis represents PrP^C levels measured with TR-FRET; the y-axis represents the number of assays grouped for the given FRET range. Controls showed a

strong separation allowing reliable detection of changes in PrP^C levels. Most of the sample population did not show a significant regulation when compared to the non-targeting controls. (D) Z' factor of each plate from the primary screen reporting the separability between the positive and negative controls. (E) Duplicate correlation over all the samples from the primary screen. The Pearson correlation coefficient, r^2-value, is depicted in the graph. (F) Volcano plot displaying -$\log_{10}$p-value and SSMD scores across the whole genome dataset. 743 candidates identified in the primary screen are colored in light blue. Final nine hits are colored in dark blue and labelled.

https://doi.org/10.1371/journal.ppat.1010013.g001

Hit validation through secondary screens

Off-target effects are a common caveat of siRNA screens and can arise because siRNA seed sequences may display homology to illegitimate loci in the genome [26,27]. In order to address this potential problem, we performed a secondary deconvolution screen. Whilst the primary screen had been performed using mixtures of three siRNAs against each gene, in the secondary screen each candidate was subjected to the three targeting siRNAs individually in U251-MG cells. Each experiment was run in three replicates, leading to 9 assays per gene for all 743 candidate genes from the primary screen. The screen was run in two subsets of genes: a first round encompassing 583 genes (Fig 2A, black dots) and a second round consisting of 160 genes (Fig 2A, purple dots). To add stringency and robustness to this approach, the same single-siRNA screen was performed with a second human cell line, GIMEN, which was chosen for its neuroectodermal origin [28] and high endogenous PrP^C expression.

Both single-siRNA screens were carried out similarly to the primary screen, except that each assay was run as a triplicate rather than duplicate. Hits were called if $\geq$ 2 of the 3 siRNAs had a strong effect (SSMD $<$ -4 or SSMD $>$ 4 or $p < 10^{-15}$). Using these criteria, we identified 54 hits (excluding *PRNP*) in U251-MG cells (Fig 2A and 2B), of which 31 were confirmed in GIMEN cells (S2 Table). Out of the 54 hits, 22 and 32 genes were classified as stabilizers and limiters, respectively.

Validation of the hits with siRNAs in smNPC-derived human neurons

PrP^C is highly expressed in human neurons [29], which are key players in prion diseases [30]. We therefore tested the 54 hits in neurons derived *in vitro* from small molecule neural progenitor cells (smNPCs) [31]. Firstly, we assessed the endogenous expression of PrP^C in smNPCs and smNPC-derived neurons at 11 days post differentiation. smNPCs and smNPC-derived neurons showed detectable levels of PrP^C (S1B Fig). We then tested the efficiency of siRNA transfection. Four-day old smNPC-derived neurons were transfected individually with three distinct *PRNP* targeting and one non-target siRNAs (10 nM). On day 11, cells were harvested and PrP^C levels were assessed by immunoblotting. The three siRNAs showed variable effects on PrP^C suppression (S1C Fig) similarly to the secondary screening, where *PRNP* siRNA 3 also showed the weakest effect.

We then investigated whether the 54 hits identified in the secondary screen produced similar effect in smNPC-derived neurons. We opted to test the effect of each gene by pooling three siRNAs, analogous to the primary whole-genome screen. siRNAs targeting the 54 hits, *PRNP*-targeting siRNAs and non-targeting siRNA controls were reformatted in a 96-well plate. smNPC-derived neurons were seeded in a separate 96-well plate and cells were transfected with siRNAs after 4 days of differentiation.

Seven days later, cells were lysed, and lysates were applied to TR-FRET readout (Fig 2C). We found that 14 targets showed a conserved effect in smNPC-derived neurons. Of these, 13 were stabilizers and one was a limiter.

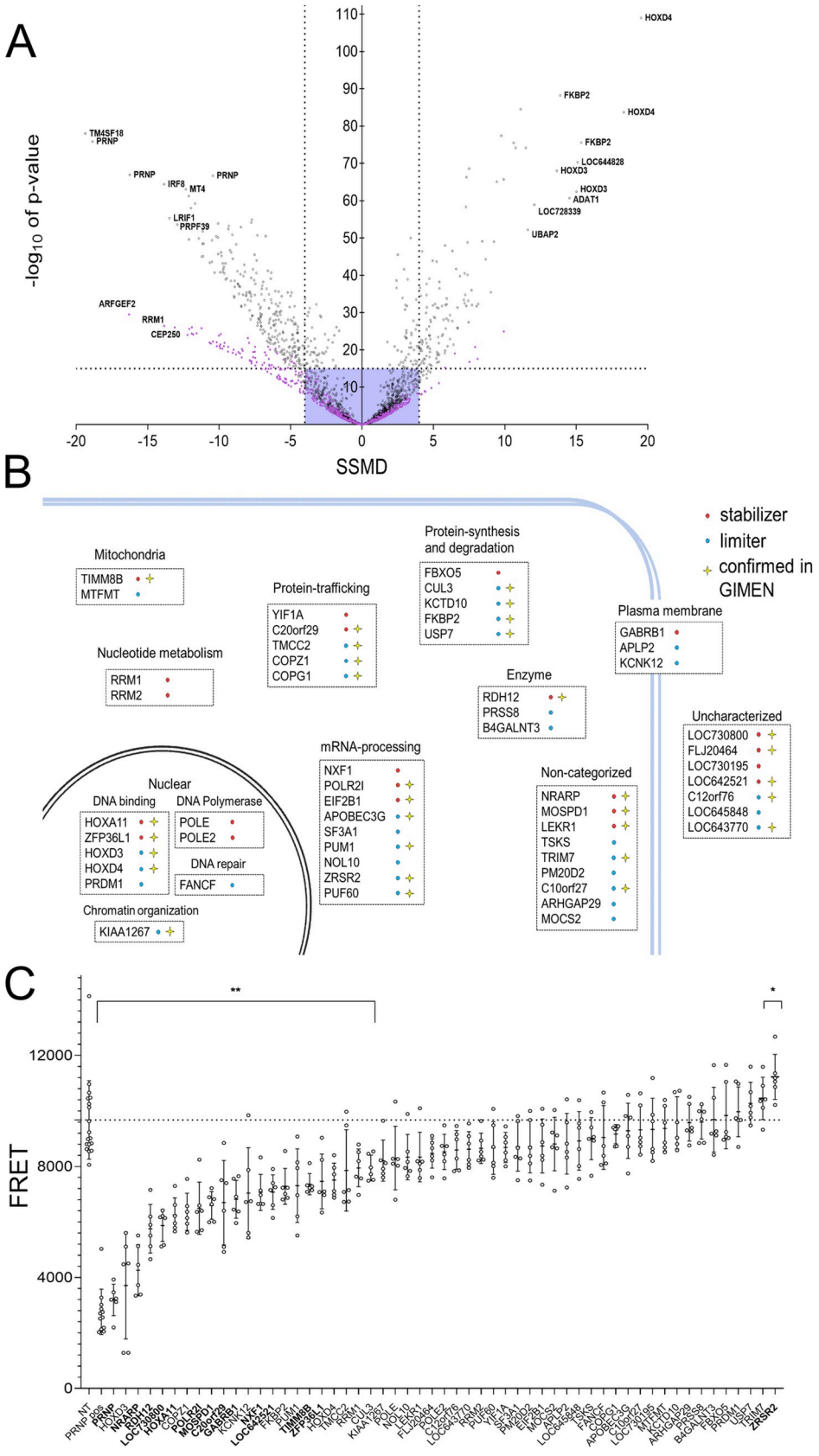
A
-log10 of p-value
SSMD
HOXD4
FKBP2
HOXD4
FKBP2
LOC644828
HOXD3
HOXD3
ADAT1
LOC728339
UBAP2
TM4SF18
PRNP
PRNP
IRF8
PRNP
MT4
LRIF1
PRPF39
ARFGEF2
RRM1
CEP250
B
stabilizer
limiter
confirmed in GIMEN
Mitochondria
TIMM8B
MTFMT
Protein-trafficking
YIF1A
C20orf29
TMCC2
COPZ1
COPG1
Protein-synthesis and degradation
FBXO5
CUL3
KCTD10
FKBP2
USP7
Plasma membrane
GABRB1
APLP2
KCNK12
Nucleotide metabolism
RRM1
RRM2
Enzyme
RDH12
PRSS8
B4GALNT3
Uncharacterized
LOC730800
FLJ20464
LOC730195
LOC642521
C12orf76
LOC645848
LOC643770
Nuclear
DNA binding
HOXA11
ZFP36L1
HOXD3
HOXD4
PRDM1
DNA Polymerase
POLE
POLE2
DNA repair
FANCF
Chromatin organization
KIAA1267
mRNA-processing
NXF1
POLR2I
EIF2B1
APOBEC3G
SF3A1
PUM1
NOL10
ZRSR2
PUF60
Non-categorized
NRARP
MOSPD1
LEKR1
TSKS
TRIM7
PM20D2
C10orf27
ARHGAP29
MOCS2
C
FRET
**
*
12000
8000
4000
0
NT
PRNP
PRNP
HOXD3
NRARP
RDH12
LOC730800
HOXA11
CUL7
FOLR3
MOSPD1
C20orf29
GABRB1
RCN1
NXF1
LOC642521
FKBP2
PUM1
TIMM8B
ZFP36L1
HOXD4
TMCC2
RRM1
CUL3
KIAA1267
POLE
NOL10
LEKR1
FLJ20464
POLE2
C12orf76
LOC645848
PUF60
RRM2
YIF1A
SF3A1
PM20D2
EIF2B1
MOCS2
APLP2
LOC644828
TSKS
FANCF
CDPCP1
APOBEC3G
C10orf27
LOC730195
MTFMT
KCTD10
ARHGAP29
PRSS8
B4GALNT3
PRDM1
USP7
TRIM7
ZRSR2

Fig 2. Secondary screening and validation of hits in smNPC-derived neurons. (A) Extent (SSMD) and confidence (p-value) of PrP^C modulation by candidate limiters (left) and stabilizers (right). Dots represent averages of triplicates; 3 siRNAs/gene were assayed. The 10 strongest limiters and stabilizers, as well as siRNAs for *PRNP* are highlighted. Violet box: cut-off criteria. Targets with ≥2 siRNAs with |SSMD| > 4 or $p < 10^{-15}$ were considered hits (n = 54). Colors indicate screening subsets (black = first round, violet = second round). (B) Function and topology of the top 54 hits. Red: stabilizers; limiters: blue. Star: hits overlapping with GIMEN cells. (C) PrP^C levels in smNPC-derived neurons transfected with a pooled set of siRNAs (as used for the primary screen, 10 nM). Dotted line: average value for cells transfected with non-target siRNAs. Genes highlighted in bold showed the same effect observed in the siRNA screening performed in U251-MG cells. n = 6 individual wells for each set of siRNAs. Values represent mean ± SD. * p = 0.0283 ** p ≥ 0.0068 (Dunnett's multiple comparisons test).

https://doi.org/10.1371/journal.ppat.1010013.g002

CRISPRi validation of hits in dCas9-KRAB U251-MG cells

In order to increase confidence in the hits identified by the secondary screening and to eliminate false-positives due to off-target effects of the siRNAs, we performed CRISPRi experiments in U251-MG cells. We chose CRISPRi as an additional method, as it acts through a repressor domain (KRAB) fused to the Cas9 protein, therefore achieving gene regulation through inhibition of transcription [32]. Since single clones of dCas9-KRAB-expressing cells can show differential basal transcriptomic signatures [33], we generated a polyclonal bulk of U251-$MG^{dCas9\text{-}KRAB}$ cells through lentiviral transduction and kept it under blasticidin selection (10 μg/mL). Next, we constructed plasmids containing four non-overlapping guide RNAs (gRNAs) per gene of interest to achieve maximum repression. Each individual gRNA was controlled by a different housekeeping promoter (hU6, mU6, hH1 and hS7K). For control, we used two sets of each 4 gRNAs bearing non-targeting sequences with no known homology to any mammalian genes. Positive control contained a construct with 4 gRNAs against *PRNP* (S2A Fig).

A total of 32 genes were further assessed with CRISPRi. We opted to exclude 22 candidates from further analysis based on low abundance of transcripts in the U251-MG line or known global regulators of protein production (expression data summary can be found in S3 Table). We seeded $2x10^5$ U251-$MG^{dCas9\text{-}KRAB}$ cells in 6-well plates and transduced them on the next day with lentiviruses containing gRNAs for each of the candidate genes. At 3 days post transduction, we selected the transduced cells with puromycin (1 μg/mL) for 5 further days (S2B Fig). Lysates were then subjected to either TR-FRET to assess PrP^C levels or quantitative real-time PCR (qRT-PCR) to determine the efficiency of the CRISPRi treatment (list of all primers used in the study can be found in S4 Table). CRISPRi yielded efficient downregulation of 27 candidates after 5 days of selection (Figs 3A and 3B and S2C, for two genes ran independently). *NXF1*, a nuclear export factor involved in mRNA export [34] did not yield an apparent downregulation potentially due to its interference with the house keeping gene, however, PrP^C levels were altered. Ten of the 32 tested hits were found to regulate PrP^C in CRISPRi experiments (Figs 3A and S2C). These ten hits were additionally assessed using western blotting as an independent method, using two antibodies targeting different epitopes. Western Blotting confirmed the regulation of PrP^C levels (Fig 3C). Interestingly, PUF60, COPG1, COPZ1 and SF3A1 seem to also affect glycosylation of PrP^C (Figs 3C and S2D).

Mechanism of action of PrP^C regulators

The hits described here may regulate PrP^C by affecting its transcription, its translation, or its turnover. In order to distinguish between these scenarios, we challenged the ten hits with CRISPRi, to additionally assess mRNA levels of *PRNP* using qRT-PCR, in combination with PrP^C levels by Western blotting and TR-FRET. KANSL1 did not reach statistical significance and was excluded from further analyses (S3A Fig). This final selection round yielded APLP2,

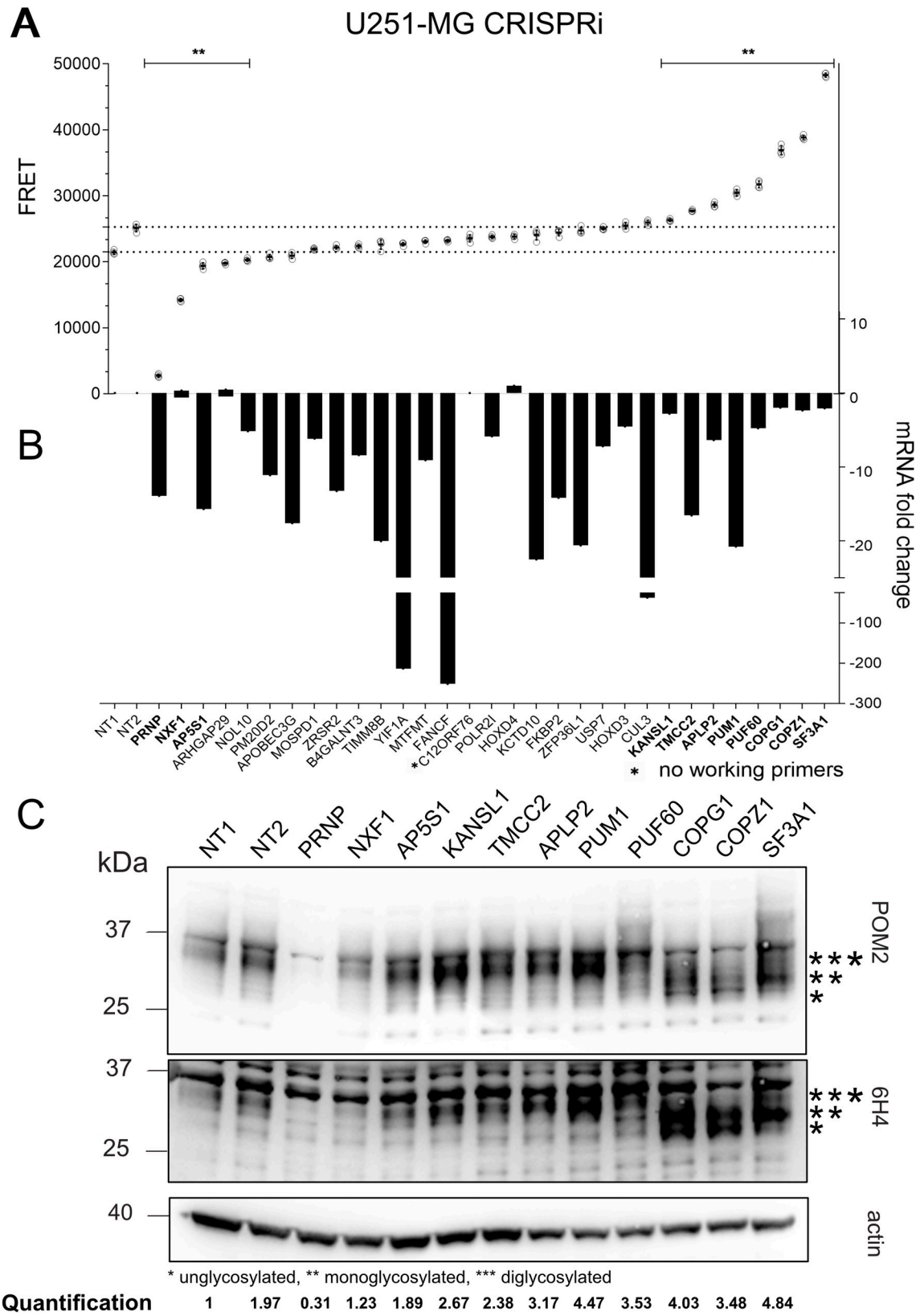

Fig 3. Hit validation in U251-MG cells by CRISPR interference. (A) PrP^C protein levels of dCas9-KRAB-U251-MG cells transduced with gRNA CRISPRi lentiviruses against the targets depicted in B. Mean values ± SD (n = 4 technical replicates) are shown. **

$p \geq 0.0023$ (Dunnett's multiple comparisons test). (B) CRISPRi activity measured by the mRNA level of the target gene in comparison to a negative control sample (NT1) after normalization to the housekeeping gene *ACTB*. *C12orf76* could not be tested due to non-functional primers. Three targets showed an increase in mRNA levels, and 27 genes showed the expected decrease in mRNA levels. Two constructs bearing non-targeting gRNAs were used for control. Only genes which showed a statistically significant difference to both NTs were considered to be true hits. Hits with same directionality and effect obtained in the siRNA screens are highlighted in bold. Bars represent averages of three replicates. (C) Western blot analysis of the ten significant samples as in A, probed with antibody 6H4 and POM2 against PrP^C. The FRET and immunoblot results were congruent. In addition, PUF60, COPZ1, COPG1 and SF3A1 induced a shift in the glycosylation pattern of PrP^C. For quantification, signal intensity of PrP^C was normalized to the signal intensity of β-actin and compared to NT1.

https://doi.org/10.1371/journal.ppat.1010013.g003

TMCC2, C20orf29/AP5S1, SF3A1, COPZ1 as post-translational regulators of PrP^C. COPG1 was found to change PrP^C levels transcriptionally and post-translationally. Instead, PUM1, PUF60 and NXF1 were found to regulate PrP^C by altering *PRNP* mRNA levels (S3B and S3C Fig). In addition, the band patterns on Western blots confirmed that CRISPR interference with PUF60, COPZ1, COPG1 and SF3A1 affected the glycosylation of PrP^C as seen in Fig 3C (S3D Fig). We conclude that CRISPRi induced highly efficient and selective repression of selected genes, thereby representing a valid tool for the independent confirmation of the results obtained from RNAi experiments.

Role for genes that regulate PrP^C expression in sporadic Creutzfeldt-Jakob disease (sCJD) susceptibility

We tested for a role of genes identified in the primary screen (n = 743) or after hit validation (n = 9) in genetic susceptibility to sCJD using data from a recent collaborative genome-wide association study [35]. Gene based tests, such as those implemented with MAGMA and VEGAS packages [36,37], aggregate single nucleotide variants within entire genes into a single statistical test, whilst accounting for linkage disequilibrium and other confounders like gene size. No genes surpassed thresholds that consider multiple testing (S5 Table). The top ranked association from the primary screen was *MPPED1* (MAGMA unadjusted p = 0.0017), and from the validated hits, *SF3A1* (MAGMA unadjusted p = 0.024).

CRISPRa validation of hits in dCas9-VPR U251-MG cells

To assess whether an opposing regulation could be achieved through the activation of the final 9 hits, we performed CRISPRa. In contrast to a repressor domain used in CRISPRi experiments, the endonuclease deficient Cas9 (dCas9) in this instance is coupled to a transcriptional activator domain, VP64-p65-RTA (VPR), leading to efficient activation of target genes [38]. In a similar setup to the CRISPRi experiments, we generated a polyclonal bulk of U251-$MG^{dCas9\text{-}VPR}$ cells and later transduced these cells using four gRNAs per gene targeting the nine hits. We included *PRNP* targeting control gRNAs as well as scrambled non-targeting gRNA sequences.

Differentially to the CRISPRi experiments, CRISPRa led to an efficient upregulation of *PRNP* on protein and mRNA levels already at three days post-selection (S4A–S4C Fig). All 9 hits were efficiently upregulated in mRNA levels as measured by qRT-PCR (S4D Fig) with at least one construct targeting different transcription start site (TSS). TMCC2, APLP2, PUM1, COPG1, COPZ1 and SF3A1 led to regulation of PrP^C measured with TR-FRET and visualized with immunoblotting in the opposing direction to the CRISPRi results (S4E and S4F Fig), suggesting these 6 hits have a bidirectional effect on PrP^C levels.

PUM1 mediates decay of *PRNP* through binding its 3'UTR

One of the 9 hits was Pumilio-1 (PUM1), an RNA-binding protein that binds its targets through their 3'-untranslated Region (3'-UTR) and mediates their decay [39]. PUM1 binds its

targets through a well-established consensus sequence, the Pumilio responsive element (PRE, 5'-UGUANAUA-3') [40]. We first tested whether the PRE was present on the 3'UTR of *PRNP*. Using the RPI-Seq tool [41], we identified a PRE within the 3'UTR of *PRNP*. To confirm that PUM1 is a regulator of *PRNP* mRNA, we performed independent siRNA transfections in 6-well plates in both cell lines, U251-MG and GIMEN. We then subjected the extracted RNA to real-time quantitative PCR (qRT-PCR) and cell lysates to immunoblotting. In both cell lines tested, we confirmed that PUM1 silencing had an upregulating effect on *PRNP* mRNA, which also resulted in higher protein levels (Fig 4A and 4B).

We then used a dual-luciferase reporter assay to test whether the effect observed was due to the predicted interaction of PUM1 with the 3'-UTR of *PRNP* mRNA. The wild-type (wt) and a mutated (mut) version of the *PRNP* 3'-UTR were cloned into pmirGLO vectors encoding Renilla and Firefly luciferase. These two enzymes report transfection efficiency and activity of the inserted construct, respectively. The mutation induced spanned three base pairs (bp) of the PRE on *PRNP* 3'-UTR to impair the binding of PUM1 as previously reported [42]. Plasmids were then transfected into HEK293T cells in presence or absence of either NT or PUM1 targeting siRNAs. Luminescence arising from the Firefly luciferase was measured after 48 hours and was followed by the measurement of Renilla luciferase for normalization. In the absence of siRNAs as well as in presence of NT siRNA treatment the mutated 3'-UTR containing construct yielded a higher signal in comparison to the wt 3'-UTR containing construct. When cells were treated with PUM1 targeting siRNAs the difference seen in the decrease in signal for the wild-type construct was abolished, indicating that PUM1 is indeed acting on the 3'-UTR of *PRNP* mRNA (Fig 4C).

Discussion

The concentration of PrP^C in any given cell type depends on an equilibrium between its biosynthesis and degradation rates, which in turn are controlled by a multitude of processes–from mRNA transcription to co-translational secretion into the endoplasmic reticulum, quality control of folding, glycolipid bonding, vesicular transport, and eventually proteolysis as well as extracellular shedding. Most factors controlling these steps are unknown, and it is difficult to imagine that they could be discovered through educated guesses. Conversely, an unbiased interrogation of the entire human genome would yield PrP^C regulators that may not have been predicted by existing knowledge.

As *PRNP* is highly expressed in the CNS [29], we chose a glioblastoma cell line U251-MG for the initial round of screening, additionally due to the suitability of this cell line in high-throughput screenings [20]. Our strategy relied on recursive screening rounds leading to progressive attrition of candidates. The primary screening campaign, in which each gene was targeted with a mixture of 3 siRNAs, identified 743 presumptive candidate genes strongly influencing PrP^C levels. However, a secondary screen with individual siRNAs showed that many of these hits could only be confirmed with one or two of the three siRNAs present in the original mixtures. These discrepancies may arise because the efficacy of suppression by the individual siRNAs was variable, or because some siRNAs exerted spurious off-target effects. We therefore decided to perform tertiary screens on those candidates that showed an effect with at least 2 siRNAs. This filtering strategy represents a trade-off between the elimination of false-positive signals and the retention of assay sensitivity.

While overexpression of some of targets may inhibit or enhance the expression of PrP^C, our screen has identified genes whose suppression would modify PrP^C expression. We therefore opted to use the terms "stabilizers" and "limiters". The resulting list of 54 stabilizers and limiters was interrogated further to assess their effect on human neurons differentiated in vitro.

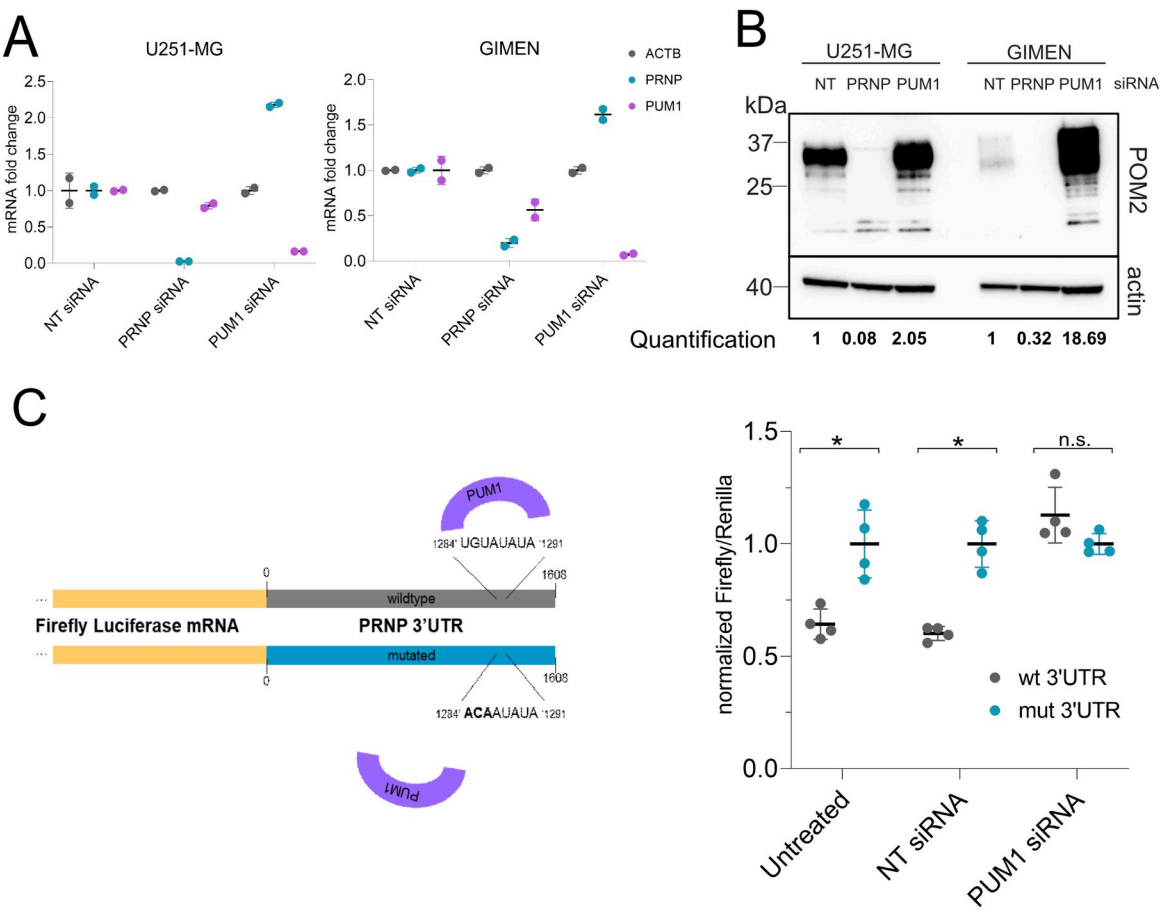

Fig 4. PUM1 regulates *PRNP* mRNA via its 3'UTR. (A) qRT-PCR analysis of U251-MG and GIMEN cell lines upon transfection with PUM1 siRNA in 6-well format. PUM1 mRNA was efficiently downregulated. ΔCt values were normalized to those of β-actin (*ACTB*). Downregulation of PUM1 resulted in increased *PRNP* mRNA in both cell lines. NT (non-targeting) and *PRNP* siRNA were used as controls. (B) Western blot analysis of U251-MG and GIMEN cell lines upon transfection with *PUM1* siRNA. PUM1 downregulation led to an upregulation of PrP^C levels (as seen in Fig 3B through CRISPRi). Antibody POM2 was used for detection of PrP^C. *PRNP* siRNA were used as controls. For quantification, signal intensity of PrP^C was normalized to the signal intensity of β-actin (C) Dual-Glo Luciferase assay to assess regulation of *PRNP* mRNA by PUM1 via its 3'-UTR. Left panel shows a schematic of the assay. The numbers indicate the position in the 3'-UTR of *PRNP*. The *PRNP* 3'-UTR sequence, predicted to bear the consensus sequence for PUM1 binding, was placed after the gene coding for the firefly luciferase. Through a mutation in the 3'-UTR binding site of PUM1 (wt 3'-UTR = > mut 3'-UTR), the binding is prevented leading to increased expression of the firefly luciferase. Two plasmids (wt 3'-UTR and mut 3'-UTR) were co-transfected into HEK293-T cells either with none, NT, or *PUM1* siRNAs. Cells transfected with the mut 3'-UTR plasmid showed a higher signal in the assay in comparison to transfection with the wt 3'UTR plasmid. Similar results were obtained for co-transfection of mut 3'-UTR plasmid and a non-targeting siRNA. The co-transfection with *PUM1* siRNA abrogated the signal difference. Means ± SD (n = 4). * $p \leq 0.016$, n.s. = non-significant (multiple t-test). NT: non-targeting siRNA.

https://doi.org/10.1371/journal.ppat.1010013.g004

These investigations confirmed that most hits were PrP^C stabilizers whereas only one was identified as a limiter. The bias towards stabilizers may be a consequence of the long half-life of proteins in post-mitotic neurons [43] which may conceal the effects of short RNAi regimens, and suggests that most stabilizers may directly affect *PRNP* biosynthesis. We addressed these questions by suppressing the genes of interest with an independent methodology. CRISPRi has recently emerged as a potent tool to reliably control gene expression [32,44]. We used multiple gRNA sequences per target, with the intent to increase the efficiency of modulation [45]. Through CRISPRi we identified nine hits significantly regulating PrP^C, six of which controlled PrP^C levels post-translationally (S6 Table).

The partial discordance between the results obtained through siRNAs and CRISPRi is not unexpected. Firstly, the mode-of action of the methods chosen are distinct from each other. In our setup, we applied siRNAs for a duration of three days, which leads to an acute depletion of the target mRNAs, however, to achieve efficient CRISPRi, the cells were cultured for eight days, during which compensatory mechanisms controlling gene expression may take place. Secondly, the use of two non-targeting controls for CRISPRi as opposed to one non-targeting control for siRNAs increases the stringency for calling hits. Thirdly, potential off-target effects seen through one of the methods can be distinct from the other.

Because of the reasons expounded above, the nine genes identified in both approaches represent, with a high degree of confidence, true regulators of PrP^C. To explore if the regulation of PrP^C by the final hits occurs bidirectionally, we made use of a second system, CRISPRa, relying on an endonuclease deficient Cas9 coupled to a transcriptional activator domain consisting of VP64-p65-RTA (VPR) [38]. We found that 6 of the 9 hits acted in an opposing direction on PrP^C levels, upon their activation with CRISPRa. One of the latter hits, Pumilio 1 (PUM1), is a known mediator of degradation of transcripts through binding to the 3'UTR on their mRNA [39]. *PRNP* was not identified in a previous study of PUM1-regulated genes [40], perhaps because of insufficient levels of PrP^C expression in HEK cells. Sequence inspections then revealed the PUM1-binding consensus sequence in the human, but not mouse, *Prnp* 3'UTR, and mutational analyses of the consensus sequence confirmed the mechanism of this regulation. The effect of PUM1 regulation on PrP^C levels was higher in GIMEN cells than in U251-MG cells, potentially due to the higher expression of PUM1 in these cells [46]. Besides clarifying the molecular mechanism by which PUM1 modulates PrP^C, these data provide direct evidence for the validity of the regulators identified in our screen.

We failed to identify any transcription factors specifically controlling PrP^C expression in the CNS, perhaps because transcriptional gene regulation relies on redundant factors. Also, the cancer cell line used for the primary screen, while derived from a CNS tumor, may not be representative of transcriptional regulation within the CNS.

Some of the regulators identified in this screen were not entirely unexpected. The members of the COPI complex, COPG1 and COPZ1, are involved in the retrograde transport of vesicles from the Golgi apparatus to the ER. Interference with the COPI complex is known to affect the expression of membrane proteins such as APP [47]. Furthermore, AP5S1 is part of the newly described Fifth Adaptor Protein Complex (AP-5) which recycles proteins out of late endosomes [48]. The decrease of PrP^C after AP5S1 knockdown may be due to decreased retrieval from late endosomes.

Other regulators were entirely unexpected, and their mechanism of action is not obvious. The ablation of APLP2 had no significant effect on incubation times of scrapie in mice [49], suggesting that the upregulation of PrP^C upon APLP2 knockdown may be specific to humans. Mechanistically, APLP2 might serve as a co-receptor for the endocytosis of PrP^C, akin to what has been described for MHC class I molecules [50] Alternatively, the regulation of PrP^C may be related to the role of APLP2 in metal homeostasis [51,52]. TMCC2 has been previously described as an ER-resident molecule that interacts with APP and has an effect on metabolism of amyloid-β [53]. In view of the analogies between prion diseases and Alzheimer's disease [54], the regulation of PrP^C via TMCC2 may occur through a common mechanism. NXF1 and PUF60, well known RNA-regulating proteins, may directly influence the availability of *PRNP* mRNA. Finally, in the case of SF3A1, a splicing factor, the regulation of PrP^C may be indirect as there are no known mechanisms by which SF3A1 could interfere with the formation of PrP^C at the protein level. Another possible mechanism of action of the hits working post-translationally, could be through enhancing or limiting shedding or cleaved products of PrP^C. To extend the understanding of the regulatory network of PrP^C expression, we also cross-

referenced the nine hits to miRNAs hits previously identified by our group [20]. The study identified four miRNA targets for which no direct interaction with *PRNP* mRNA was established. However, based on the target prediction data, miRDB, [55] we did not find any plausible links between the identified miRNA hits and the nine hits reported here.

In addition to the mechanisms discussed above, the biogenesis of PrP^C involves co-translational secretion of the nascent polypeptide chain into the lumen of the ER and addition of a glycophosphoinositol (GPI) anchor. However, not all of the players known to control these processes were identified as hits. For one thing, some of these genes encode essential proteins whose knockdown may drastically decrease cell viability. Furthermore, because the pathways involved in proteostasis are multiple and partially redundant [56], suppressing a single gene may not result in a measurable effect on PrP^C levels.

In many neurodegenerative diseases, including Alzheimer's and Parkinson's disease, fundamental clues to the pathogenesis were provided by the study of families with Mendelian disease transmission. However, in the case of prion diseases these strategies have been largely unsuccessful. Although genome-wide association studies (GWAS) have identified two potential risk loci [35], the only strong genetic risk factor for Creutzfeldt-Jakob disease has remained *PRNP* itself [57]. This sobering situation was a primary driver of the present study, as the assessment of every individual protein-coding genes may plausibly highlight factors undetectable by human genetics. In addition, we did not find evidence of a genetic association between screen hits and sCJD susceptibility using gene-based analysis from a recent GWAS [35]. Similarly, in the GWAS, PrP brain expression quantitative trait loci near to *PRNP* showed no evidence of association with sCJD. Expression level of PrP is a powerful determinant of incubation time in rodent models of prion disease [58], but overexpression does not appear to effect susceptibility to infection [59]. Whether the genetic regulators of PrP expression in cells determine aspects of the phenotype of the human disease such as age at onset or clinical duration remains to be determined. The ranked genetic associations of the screen hits made available here may be useful in prioritization of genes for future studies. The modifiers enumerated here provide unexpected insights into a vast and highly diverse regulatory network of PrP^C, and may eventually provide druggable targets for development of therapeutics in addition to the direct suppression of PrP^C [60,61], for instance through mRNA-based therapeutics to modulate PrP^C-limiters [62].

Material and methods

Cell culturing

U-251MG human cells (Kerafast, Inc., Boston, MA, USA, AccessionID: CVCL_0021) and GIMEN human cells (CLS Gmbh, Eppelheim, Germany AccessionID: CVCL_1232) cells were cultured in T150 tissue culture flasks (TPP, Trasadingen, Switzerland) in OptiMEM without Phenol (Gibco, Thermo Fisher Scientific, Waltham, MA, USA) supplemented with 10%FBS (Takara, Göteborg, Sweden), 1% NEAA (Gibco), 1% GlutaMax (Gibco), and 1% Penicilin/Streptomycin (P/S) (Gibco). HEK293-T cells (Human embryonal kidney, AccessionID: CRL_3216) were cultured DMEM without phenol (Gibco) with the same conditions for aforementioned supplements. In preparation for the screening, cells were expanded, either harvested using Trypsin-EDTA 0.025% (Gibco) or Accutase (Gibco), washed with PBS (Kantonsapotheke, Zurich, Switzerland) and resuspended in Penicilin/Streptomycin free medium, pooled, and counted using TC20 (BioRad) Cell Counter with trypan blue (Gibco). Culturing and differentiation of smNPC-derived human neurons was performed as described [31].

siRNA library preparation and reformatting

Whole genome Silencer Select Human Genome siRNA Library V4 (Thermo Fisher Scientific), which includes three individual siRNAs targeting each gene (64752 total siRNAs targeting 21.584 human genes) was purchased at the quantity of 0.25 nmol. Upon delivery, the lyophilized library was resuspended in RNAse free water (Thermo Fisher Scientific) to a final concentration of 5 μM. siRNAs targeting the same gene were aliquoted in a single transfer step using ViaFlo equipment (Integra, Konstanz, Germany) either as pooled siRNAs (referred to as the pooled library) targeting the same gene or as single siRNAs (referred to as the single library) into ECHO acoustic dispenser (Labcyte, San Jose, CA, USA) compatible 384-well LDV plates (Labcyte). For the primary screen, pooled siRNAs and control siRNAs were dispensed in duplicates at a final concentration of 5 nM (20 nM for Cell Death control, Qiagen, Hilden, Germany) into white 384-well CulturPlates (Perkin Elmer, Beaconsfield, UK) using an ECHO 555 acoustic dispenser according to an optimized plate layout [20] and stored at -40˚C until further use. For the secondary screen, individual siRNAs were dispensed in triplicates. As controls, a scrambled non-targeting siRNA (NT) (Ambion, Thermo Fisher Scientific) as negative and a PRNP targeting siRNA (Ambion, Thermo Fisher Scientific) as positive control, were reformatted to destination plates either as three siRNAs in pooled format or as single siRNAs. All siRNA sequences are accessible under the PubChem repository, NCBI [63].

Screening workflow

Cell culture plates containing reformatted siRNAs were thawed and 5 μL RNAiMAX (Invitrogen, Carlsbad, CA, USA) (1.8% v/v, final conc. 0.3%) diluted in P/S free medium was dispensed using a multi-drop dispenser (MultiFlo FX, Biotek, Vinooski, VT, USA). Plates were centrifuged at 1000xg for 1 minute (Eppendorf 5804R, Hamburg, Germany) and incubated for 30 min at room temperature (RT). Afterwards, 6'000 cells (U251-MG) or 8'000 cells (GIMEN) per well were seeded in 25 μL P/S free medium and plates were incubated in a rotating tower incubator (LiCONiC StoreX STX, Schaanwald, Liechtenstein). For the primary screen, plates were removed from the incubator after 70 hours and 10 μL of 4x RT-Glo substrate and enzyme per well (Promega, Madison, WI, USA) diluted in P/S free medium, was added. Plates were incubated for another 2 hours in the incubator. Prior to measuring luminescence temperature of EnVision plate reader (Perkin Elmer) was set to 37˚C and luminescence was measured without disturbances in temperature. Subsequently, medium was removed by inverting the plates, and cells were lysed in 10 μL lysis buffer (0.5% Na-Deoxycholate (Sigma Aldrich St. Louis, MO, USA) 0.5% Triton X (Sigma Aldrich), supplemented with EDTA-free cOmplete Mini Protease Inhibitors (Roche, Basel, Switzerland) and 0.5% BSA (Merck, Darmstadt, Germany). Following lysis, assay plates were incubated on a plate shaker (Eppendorf ThermoMixer Comfort) for 10 min (4˚C, 700 rpm shaking conditions) prior to centrifugation at 1000xg for 1 min and incubated at 4˚C for two additional hours. Following incubation, plates were centrifuged once more under same conditions mentioned above and 5 μL of each FRET antibody pair was added (2.5 nM final concentration for donor and 5 nM for acceptor, diluted in 1x Lance buffer, (Perkin Elmer)). For FRET, two distinct anti-PrP antibodies, POM1 (binding to amino acid residue (a.a) 144–152) and POM2 (binding to a.a 43–92) [64], targeting different epitopes of PrP^C were coupled to a FRET donor, Europium (EU) and a FRET acceptor, Allophycocyanin (APC), respectively, following previously reported protocols [21]. For APC–POM1 coupling, Lightning-Link APC Labeling Kit (Lucerna Chem, Lucerne, Switzerland) was used following manufacturer's instructions. Plates were centrifuged once more and incubated overnight at 4˚C. TR-FRET measurements were read out using previously reported parameters [21] on an EnVision multimode plate reader (Perkin Elmer).

Screening data analysis

Screening data was analyzed using an in-house developed, open-source, Phyton-based high throughput screen (HTS) analysis pipeline (all documentation and code available under: https://github.com/elkeschaper/hts). Net-FRET data was calculated [21] and subjected to various quality control checkpoints. Initially, a heat map of individual plates was plotted to examine temperature-induced gradients or dispensing errors. Subsequently, z'-Factor and strictly standardized mean difference (SSMD) scores [24,25] were calculated to report the robustness of the screens. Additionally, Net-FRET values were plotted to check for row or column effects as well as assessing correlation of duplicates or triplicates. After assessing quality of each individual plate, candidate genes were selected with the following cut-off criteria: SSMD of < -4 and > 4 *or* a p-value (t-test) of below 10^{-15}. After the secondary screen, same cut-off criteria were used with the additional requirement at least 2 out of 3 individual siRNAs targeting the same transcript passing the threshold. Graphs were generated with GraphPad Prism.

PUM1 validation and reporter assay

U251-MG or GI-ME-N cells were seeded into 6- well cell culture plates in a total culture volume of 1.5 mL. Next days, cells were transfected with NT or PUM1 siRNAs (Thermo Fisher Scientific) to a final concentration of 5 nM in a total culture volume of 2 mL. 72 hours post-transfections cells were washed once in PBS to remove cell debris and collected for immunoblotting and quantitative real-time polymerase chain reaction (qRT-PCR). For immunoblottings, cells were scraped with 100 μL lysis buffer (50 mM Tris-HCl pH 8, 150 mM NaCl, 0.5% sodium deoxycholate, 0.5% Triton-X 100, Sigma) supplemented with EDTA-FREE cOmplete Mini protease inhibitor cocktail (Sigma), incubated on ice for 20 minutes and centrifuged at 10.000xg for 10 minutes for isolation of proteins. Supernatants were then subjected to bicinchoninic acid assay (BCA) (Pierce, Waltham, MA, USA) to measure total protein concentrations according to manufacturer's instructions. 25 μg of total proteins of all samples were loaded onto a 4–12% gradient gel (Invitrogen) and blotted onto a PVDF membrane (Invitrogen). Following blocking in 5% SureBlock reagent (LubioScience, Zurich, Switzerland) diluted in PBS-Tween20 (PBST, Sigma) for 30 minutes, anti-PrP antibody POM2 [64] was applied to the membrane at a final concentration of 300 ng/mL in 1% SureBlock in PBST and incubated overnight at 4˚C. As a detection antibody anti-Mouse HRP (BioRad) was used diluted 1:10.000 in 1% SureBlock containing PBST. Immunoblots were developed with Crescendo HRP substrate (Millipore, Dachstein, France). As loading control, an anti-Actin antibody m25 (Merck) was used at a dilution of 1:10.000 in 1% Sureblock containing PBST. Imaging was performed on Vilber (Eberhardzell, Germany) systems. Quantification was done with ImageLab (BioRad) For qRT-PCR, cells were lysed in 350 μL RLT lysis buffer (Qiagen) and RNA was extracted using RNeasy Mini kit (Qiagen) manufacturer's instructions. Concentration and quality of RNA was assessed using a NanoDrop spectrophotometer (Thermo Fisher Scientific). cDNA synthesis was done following the manufacturer's instructions using the Quantitect Reverse Transcription kit (Qiagen). A total of 25 ng of cDNA per sample was manually transferred into 384-well PCR plates (Thermo Fisher Scientific) and SYBR green (Roche) mastermix was used for detection. Readout was performed with ViiA7 Real Time PCR systems (Thermo Fisher Scientific). As internal controls, three housekeeping genes (ACTB, TBP, GUSB) were measured for each sample. Data was analyzed and visualized using GraphPad Prism.

Wild-type 3'UTR of PRNP (1608 base pairs (bp)) and a mutant version thereof, were ordered as gene blocks (Integrated DNA Technologies (IDT), Newark, NJ, USA). The mutation was positioned at the PUM1 binding site 5'-TGTATATA-3', where TGT was exchanged to ACA in line with previous reports [42]. Additionally, the sequence was modified to contain

an overlap of 25 bp at the 5' end and 21 bp at the 3' end with the pmirGLO Dual-Luciferase miRNA Target Expression Vector for molecular cloning into pmirGLO Dual-Luciferase miRNA Target Expression Vector (Promega). The pmirGLO vector was initially digested with PmeI (New England Biolabs (NEB), Ipswitch, MA, USA) and SalI (NEB). Either the wild-type or the mutant version of the *PRNP* 3'UTR were inserted into the digested pmirGLO vector by performing a Gibson Assembly following manufacturer's instructions (NEB). After transformation of the cloned vectors and purification of the DNA using EndoFree Plasmid Maxi Kit (Qiagen), the purified products were sent to Microsynth AG (Balgach, Switzerland) for Sanger sequencing and aligned to reference sequence of 3'UTR of *PRNP* using Nucleotide-Blast (NCBI). Final constructs were designated as wild-type (wt)-3'UTR-pmirGLO or mutant (mut)-3'UTR-pmirGLO.

$1x10^4$ HEK-293T cells were seeded in culture medium without antibiotics in white 96-well culture plates (Perkin Elmer) prior to transfection. 100 ng of the wt/mut- 3'UTR-pmirGLO plasmid and 1 pmol of PUM1 or NT siRNAs (Thermo Fisher Scientific) were co-transfected in quadruplicates for each condition using 1% Lipofectamine 2000 (Thermo Fisher Scientific). Four additional wells contained no siRNAs. 48 hours post-transfection, the Dual-Glo Luciferase Reagent (Promega) was added to each well and the luminescence of the firefly luciferase was measured using EnVision plate reader (Perkin Elmer) after 20 min incubation at RT. Subsequently, Dual-Glo Stop & Glo Reagent diluted (1:100) in culture medium (Promega) was added to each well and the luminescence of the renilla luciferase was measured after 20 min incubation at RT. For data analysis, the Firefly luciferase signal was normalized to the renilla luciferase signal and statistical significance was determined through a t-test and plotted using GraphPad Prism. All sequences for primers can be found in the S4 Table.

CRISPRi and CRISPRa in dCas9-U251-MG

The plasmid encoding Lenti-dCas9-KRAB-blast for CRISPRi was a gift from Gary Hon (Addgene plasmid #89567; http://n2t.net/addgene:89567) and the plasmid for CRISPRa was acquired from Addgene (plasmid #96917; https://www.addgene.org/96917/). The plasmids were packaged into a lentivirus and U251-MG were transduced with 200 μL of each virus. Two days later, blasticidin (Gibco) at a concentration of 10 μg/mL was supplied to the culture medium and cells were continuously kept under antibiotic selection and the resulting clonal cells are denoted as dCas9-KRAB U251-MG for CRISPRi and dCas9-VPR U251-MG for CRISPRa. Plasmids containing guide RNAs (gRNAs) against each target were produced and lentivirally packaged. After 10 days of selection with blasticidin (Gibco) containing medium, 200.000 dCas9-KRAB U251-MG or dCas9-VPR U251-MG cells were seeded into a 6-well plate. One day later, cells were transduced with 15 μL of viruses containing the gRNAs against each target. As controls, two different NT constructs for CRISPRi and one for CRISPRa and a *PRNP* targeting construct were used. After 72 hours for CRISPRi and 24 hours for CRISPRa, cell media was replaced with fresh medium containing 1 μg/mL puromycin (Gibco) to select for transduced cells. Cell media was replenished once more with puromycin containing medium and selection of transduced cells was terminated after a total selection duration of 5 days for CRISPRi and 3 days for CRISPRa in culture. Subsequently, cells were washed once in PBS and lysed for downstream analysis by TR-FRET and immunoblotting as well as quantitative real-time polymerase chain reaction (qRT-PCR). For TR-FRET and immunoblotting, cells were lysed by scraping in a total volume of 80 μL of lysis buffer (containing 50 mM Tris-HCl pH 8, 150 mM NaCl, 0.5% sodium deoxycholate, 0.5% Triton-X 100, Sigma) and processed for immunoblotting as described in this manuscript under the PUM1 validation subchapter. A BCA assay was used for normalization to total protein concentration prior to FRET and

Western Blot analyses. A BCA assay was used to assess the total protein concentration of the samples and the sample volume was adapted to achieve the same protein amount for subsequent FRET and Western Blot analyses. To quantitate PrP^C levels with a TR-FRET reaction the same antibodies were used as for the screening. In detail, 10 μl of lysates were manually transferred to a 384-well opaque OptiPlate (Perkin Elmer) in quadruplicate wells and supplied with APC-POM1 and EU-POM2 (5 and 2.5 nM final concentration, respectively diluted in LANCE buffer). Plates were incubated overnight at 4˚C followed by centrifugation and TR-FRET measurements were done with the same parameters used for the screening workflow. qRT-PCR was followed as described in the previous PUM1 validation section of this manuscript following the same protocol. For CRISPRi, each sample was measured for three housekeeping genes (ACTB, GUSB and TBP) for normalization as well as their own respective primers to assess efficiency. For the final 9 hits, *PRNP* mRNA was assessed as well. For CRISPRa, each sample was measured for ACTB for normalization as well as their own respective primers to assess efficiency. qRT-PCR data was analyzed using the $2^{-\Delta\Delta CT}$ method and visualized using GraphPad Prism. All primer sequences are listed under S4 Table.

RNA-Sequencing in the U251-MG cell line

RNA extraction was performed using the RNeasy Mini Kit (Qiagen) according to the manufacturer's instructions. The libraries were prepared following Illumina TruSeq stranded mRNA protocol. The quality of the RNA and final libraries was determined using an Agilent 4200 TapeStation System. The libraries were pooled equimolecularly and sequenced in an Illumina NovaSeq6000 sequencer (single-end 100 bp) with a depth of around 20 Million reads per sample. The experiment was run in triplicates. For thresholding for non-expressed or low expressed genes before CRISPRi validation, first the average normalized counts for triplicates were calculated and a cut-off value of 25 was used (S3 Table).

Supporting information

S1 Fig. Additional quality control of primary screening and establishment of siRNA treatment for smNPC-derived neurons. (A) Strictly standardized mean difference of each plate from the primary screening reporting the separation of the positive and negative controls. Range of the quality metrics (poor to excellent) is reported based on the highest level of stringency [25]. (B) Endogenous PrP^C levels in human smNPCs and smNPC-derived neurons (day 11 post differentiation) assessed through immunoblotting. U251-MG was used as a positive control. The anti-PrP antibody POM2 was used for detection of PrP^C. (C) Western blot analysis of 11 days old smNPC-derived neurons upon transfection with three distinct *PRNP* targeting siRNAs and a non-targeting siRNA as well as Lipofectamine only and untreated control. *PRNP* siRNA 1 and 2 lead to a marked decrease of PrP^C levels 6 days after transfection. (TIF)

S2 Fig. Establishment, experimental setup and results of CRISPRi in dCas9-KRAB-U251-MG cells. (A) Efficacy of CRISPRi in dCas9-KRAB-U251-MG through lentiviral transduction of a construct containing four single guides against *PRNP* as well as two non-targeting controls assessed through immunoblotting. After CRISPRi treatment followed by antibiotic selection for five days an evident reduction of PrP^C levels is apparent. (B) Schematic depicting the setup of the CRISPRi experiments in dCas9-KRAB-U251-MG cells. (C) Two candidates tested independently. PrP^C protein levels of dCas9-KRAB-U251-MG cells transduced with gRNA CRISPRi lentiviruses against both targets. Mean values ± SD (n = 4 technical replicates) are shown. CRISPRi activity measured by the mRNA level of the target gene in comparison to

a negative control sample (NT1) after normalization to the housekeeping gene ACTB. (D) Quantification of the glycosylation pattern differences in all samples indicates a shift of glycosylation of PrP^C upon regulation of PUF60, COPZ1, COPG1 and SF3A1.
(TIF)

S3 Fig. Mechanism of action of PrP^C regulators. (A) Panels depicting the effect of CRISPRi downregulation on PrP^C levels assayed using TR-FRET, as well as the on-target efficiency of CRISPRi downregulation on each target assessed by qRT-PCR. (B) Effect of CRISPRi downregulation in A assessing *PRNP* mRNA levels. *ACTB* was used as a housekeeping gene and samples were compared to non-target 1 (NT1) (C) Modulation of *PRNP* mRNA and PrP^C protein levels after CRISPRi mediated suppression of 2 stabilizers and 7 limiters. qRT-PCR and *PRNP* mRNA FRET analysis of the nine hits with a significant effect on PrP^C, in an independent repetition experiment. Samplers were normalized to *ACTB*. Three genes (pink) regulated *PRNP* mRNA levels, whereas five (blue) modulated PrP^C post-transcriptionally and one gene (pink circle with blue filling) acted both transcriptionally and post-transcriptionally. (D) Western blot analysis of same samples as in A, probed with antibody POM2 against PrP^C. FRET and immunoblot results were congruent and the shift in the glycosylation for PUF60, COPZ1, COPG1 and SF3A1 was persistent confirming the results from Fig 3C. For quantification, signal intensity of PrP^C was normalized to the signal intensity of β-actin and compared to NT1.
(TIF)

S4 Fig. Establishment, experimental setup and results of CRISPRa in dCas9VPR-U251MG cells. (A) Schematic depicting the setup of the CRISPRa experiments in dCas9-VPR-U251-MG cells. (B) Efficacy of CRISPRa in dCas9-VPR-U251-MG by lentivirally transduce a construct containing gRNAs against *PRNP* as well as a non-targeting control assessed through immunoblotting. (C) Additional quantification of B using TR-FRET. qRT-PCR of the same setup as in B. ΔCt values were normalized to those of *ACTB*. After CRISPRa treatment followed by antibiotic selection for three days an increase in PrP^C levels is apparent. (D) CRISPRa efficiency for each gene measured by qRT-PCR after selection for three days. ΔCt values were normalized to those of *ACTB*. (E) Effect of CRISPRa for all targets assayed on PrP^C levels measured by TR-FRET. (F) Western blot analysis of representative samples from E. Antibody POM2 was used for detection of PrP^C. * $p \geq 0.05$, ** $p \geq 0.01$, **** $p \geq 0.0001$, n.s. = non-significant (Dunnett's multiple comparisons test).
(TIF)

S1 Table. Whole genome-RNAi screen results. (A) Summary excel sheet for the primary screen dataset involving SSMD, log2fold change and p-values for each replicate. (B) Summary of the 743 candidates that were validated in the secondary screening round.
(XLSX)

S2 Table. Secondary Screen hits. Effect of the 55 siRNA hits in U251-MG and GIMEN.
(XLSX)

S3 Table. RNA-Seq normalized counts for U251-MG.
(XLSX)

S4 Table. Sequences of primers used in the study.
(XLSX)

S5 Table. MAGMA and VEGAS scores for the comparison of PrP^C hits and sCJD GWAS dataset.
(XLSX)

S6 Table. Summary of the final nine hits.
(XLSX)

Acknowledgments

We would like to thank Dr. Emilio Yangüez and Dr. Maria Domenica Moccia and the Functional Genomics Center Zurich (FGCZ) for their help with the RNA-Sequencing experiment. We thank Irina Abakumova and Rita Moos for their technical help.

Author Contributions

Conceptualization: Daniel Heinzer, Merve Avar, Ashutosh Dhingra, Adriano Aguzzi.

Data curation: Daniel Heinzer, Merve Avar, Daniel Patrick Pease, Ashutosh Dhingra, Berre Doğançay, Simon Mead.

Formal analysis: Daniel Heinzer, Merve Avar, Elke Schaper, Berre Doğançay, Andra Chincisan, Simon Mead.

Funding acquisition: Adriano Aguzzi.

Investigation: Daniel Heinzer, Merve Avar, Daniel Patrick Pease, Ashutosh Dhingra, Berre Doğançay.

Methodology: Daniel Heinzer, Merve Avar, Daniel Patrick Pease, Ashutosh Dhingra, Jiang-An Yin, Berre Doğançay, Marc Emmenegger.

Project administration: Daniel Heinzer, Merve Avar.

Resources: Jiang-An Yin, Elke Schaper, Marc Emmenegger, Anna Spinelli, Kevin Maggi, Adriano Aguzzi.

Software: Elke Schaper, Andra Chincisan.

Supervision: Simone Hornemann, Peter Heutink, Adriano Aguzzi.

Validation: Daniel Heinzer, Merve Avar, Ashutosh Dhingra, Berre Doğançay.

Visualization: Daniel Heinzer, Merve Avar, Adriano Aguzzi.

Writing – original draft: Daniel Heinzer, Merve Avar, Adriano Aguzzi.

Writing – review & editing: Daniel Heinzer, Merve Avar, Daniel Patrick Pease, Ashutosh Dhingra, Jiang-An Yin, Elke Schaper, Berre Doğançay, Marc Emmenegger, Anna Spinelli, Kevin Maggi, Andra Chincisan, Simone Hornemann, Peter Heutink, Adriano Aguzzi.

References

1. Aguzzi A, De Cecco E. Shifts and drifts in prion science. Science. 2020; 370(6512):32–4. https://doi.org/10.1126/science.abb8577 PMID: 33004500
2. Küffer A, Lakkaraju AK, Mogha A, Petersen SC, Airich K, Doucerain C, et al. The prion protein is an agonistic ligand of the G protein-coupled receptor Adgrg6. Nature. 2016; 536(7617):464–8. https://doi.org/10.1038/nature19312 PMID: 27501152
3. Wulf MA, Senatore A, Aguzzi A. The biological function of the cellular prion protein: an update. BMC Biol. 2017; 15(1):34. https://doi.org/10.1186/s12915-017-0375-5 PMID: 28464931
4. Brandner S, Isenmann S, Raeber A, Fischer M, Sailer A, Kobayashi Y, et al. Normal host prion protein necessary for scrapie-induced neurotoxicity. Nature. 1996; 379(6563):339–43. https://doi.org/10.1038/379339a0 PMID: 8552188

5. Bueler H, Raeber A, Sailer A, Fischer M, Aguzzi A, Weissmann C. High prion and PrPSc levels but delayed onset of disease in scrapie-inoculated mice heterozygous for a disrupted PrP gene. Mol Med. 1994; 1(1):19–30. PMID: 8790598

6. Vallabh SM, Minikel EV, Schreiber SL, Lander ES. Towards a treatment for genetic prion disease: trials and biomarkers. Lancet Neurol. 2020; 19(4):361–8. https://doi.org/10.1016/S1474-4422(19)30403-X PMID: 32199098

7. Karapetyan YE, Sferrazza GF, Zhou M, Ottenberg G, Spicer T, Chase P, et al. Unique drug screening approach for prion diseases identifies tacrolimus and astemizole as antiprion agents. Proc Natl Acad Sci U S A. 2013; 110(17):7044–9. https://doi.org/10.1073/pnas.1303510110 PMID: 23576755

8. Silber BM, Gever JR, Rao S, Li Z, Renslo AR, Widjaja K, et al. Novel compounds lowering the cellular isoform of the human prion protein in cultured human cells. Bioorg Med Chem. 2014; 22(6):1960–72. https://doi.org/10.1016/j.bmc.2014.01.001 PMID: 24530226

9. Shyu WC, Harn HJ, Saeki K, Kubosaki A, Matsumoto Y, Onodera T, et al. Molecular modulation of expression of prion protein by heat shock. Mol Neurobiol. 2002; 26(1):1–12. https://doi.org/10.1385/MN:26:1:001 PMID: 12392052

10. Vincent B, Sunyach C, Orzechowski HD, St George-Hyslop P, Checler F. p53-Dependent transcriptional control of cellular prion by presenilins. J Neurosci. 2009; 29(20):6752–60. https://doi.org/10.1523/JNEUROSCI.0789-09.2009 PMID: 19458243

11. Bellingham SA, Coleman LA, Masters CL, Camakaris J, Hill AF. Regulation of prion gene expression by transcription factors SP1 and metal transcription factor-1. J Biol Chem. 2009; 284(2):1291–301. https://doi.org/10.1074/jbc.M804755200 PMID: 18990686

12. Dery MA, Jodoin J, Ursini-Siegel J, Aleynikova O, Ferrario C, Hassan S, et al. Endoplasmic reticulum stress induces PRNP prion protein gene expression in breast cancer. Breast Cancer Res. 2013; 15(2):R22. https://doi.org/10.1186/bcr3398 PMID: 23497519

13. Parkyn CJ, Vermeulen EG, Mootoosamy RC, Sunyach C, Jacobsen C, Oxvig C, et al. LRP1 controls biosynthetic and endocytic trafficking of neuronal prion protein. J Cell Sci. 2008; 121(Pt 6):773–83. https://doi.org/10.1242/jcs.021816 PMID: 18285446

14. Rybner C, Hillion J, Sahraoui T, Lanotte M, Botti J. All-trans retinoic acid down-regulates prion protein expression independently of granulocyte maturation. Leukemia. 2002; 16(5):940–8. https://doi.org/10.1038/sj.leu.2402443 PMID: 11986958

15. Graner E, Mercadante AF, Zanata SM, Forlenza OV, Cabral AL, Veiga SS, et al. Cellular prion protein binds laminin and mediates neuritogenesis. Brain Res Mol Brain Res. 2000; 76(1):85–92. https://doi.org/10.1016/s0169-328x(99)00334-4 PMID: 10719218

16. Mantuano E, Azmoon P, Banki MA, Lam MS, Sigurdson CJ, Gonias SL. A soluble derivative of PrP. J Biol Chem. 2020; 295(41):14178–88. https://doi.org/10.1074/jbc.RA120.013779 PMID: 32788217

17. Salzano G, Giachin G, Legname G. Structural Consequences of Copper Binding to the Prion Protein. Cells. 2019; 8(8). https://doi.org/10.3390/cells8080770 PMID: 31349611

18. Uhlén M, Fagerberg L, Hallström BM, Lindskog C, Oksvold P, Mardinoglu A, et al. Proteomics. Tissue-based map of the human proteome. Science. 2015; 347(6220):1260419. https://doi.org/10.1126/science.1260419 PMID: 25613900

19. TheProteinAtlas. The Protein Atlas [Available from: https://www.proteinatlas.org/ENSG00000171867-PRNP/cell.

20. Pease D, Scheckel C, Schaper E, Eckhardt V, Emmenegger M, Xenarios I, et al. Genome-wide identification of microRNAs regulating the human prion protein. Brain Pathol. 2019; 29(2):232–44. https://doi.org/10.1111/bpa.12679 PMID: 30451334

21. Ballmer BA, Moos R, Liberali P, Pelkmans L, Hornemann S, Aguzzi A. Modifiers of prion protein biogenesis and recycling identified by a highly parallel endocytosis kinetics assay. J Biol Chem. 2017; 292(20):8356–68. https://doi.org/10.1074/jbc.M116.773283 PMID: 28341739

22. Keller A, Nuvolone M, Abakumova I, Chincisan A, Reimann R, Avar M, et al. Prion pathogenesis is unaltered in a mouse strain with a permeable blood-brain barrier. PLoS Pathog. 2018; 14(11):e1007424. https://doi.org/10.1371/journal.ppat.1007424 PMID: 30496289

23. Senatore A, Frontzek K, Emmenegger M, Chincisan A, Losa M, Reimann R, et al. Protective anti-prion antibodies in human immunoglobulin repertoires. EMBO Mol Med. 2020; 12(9):e12739. https://doi.org/10.15252/emmm.202012739 PMID: 32776637

24. Zhang JH, Chung TD, Oldenburg KR. A Simple Statistical Parameter for Use in Evaluation and Validation of High Throughput Screening Assays. J Biomol Screen. 1999; 4(2):67–73. https://doi.org/10.1177/108705719900400206 PMID: 10838414

25. Zhang XD. Illustration of SSMD, z score, SSMD*, z* score, and t statistic for hit selection in RNAi high-throughput screens. J Biomol Screen. 2011; 16(7):775–85. https://doi.org/10.1177/1087057111405851 PMID: 21515799

26. Jackson AL, Bartz SR, Schelter J, Kobayashi SV, Burchard J, Mao M, et al. Expression profiling reveals off-target gene regulation by RNAi. Nat Biotechnol. 2003; 21(6):635–7. https://doi.org/10.1038/nbt831 PMID: 12754523

27. Jackson AL, Linsley PS. Recognizing and avoiding siRNA off-target effects for target identification and therapeutic application. Nat Rev Drug Discov. 2010; 9(1):57–67. https://doi.org/10.1038/nrd3010 PMID: 20043028

28. Kuzyk A, Gartner J, Mai S. Identification of Neuroblastoma Subgroups Based on Three-Dimensional Telomere Organization. Transl Oncol. 2016; 9(4):348–56. https://doi.org/10.1016/j.tranon.2016.07.001 PMID: 27567959

29. Bendheim PE, Brown HR, Rudelli RD, Scala LJ, Goller NL, Wen GY, et al. Nearly ubiquitous tissue distribution of the scrapie agent precursor protein. Neurology. 1992; 42(1):149–56. https://doi.org/10.1212/wnl.42.1.149 PMID: 1346470

30. Mallucci GR, White MD, Farmer M, Dickinson A, Khatun H, Powell AD, et al. Targeting cellular prion protein reverses early cognitive deficits and neurophysiological dysfunction in prion-infected mice. Neuron. 2007; 53(3):325–35. https://doi.org/10.1016/j.neuron.2007.01.005 PMID: 17270731

31. Dhingra A, Täger J, Bressan E, Rodriguez-Nieto S, Bedi MS, Bröer S, et al. Automated Production of Human Induced Pluripotent Stem Cell-Derived Cortical and Dopaminergic Neurons with Integrated Live-Cell Monitoring. J Vis Exp. 2020(162). https://doi.org/10.3791/61525 PMID: 32831313

32. Qi LS, Larson MH, Gilbert LA, Doudna JA, Weissman JS, Arkin AP, et al. Repurposing CRISPR as an RNA-guided platform for sequence-specific control of gene expression. Cell. 2013; 152(5):1173–83. https://doi.org/10.1016/j.cell.2013.02.022 PMID: 23452860

33. Stojic L, Lun ATL, Mangei J, Mascalchi P, Quarantotti V, Barr AR, et al. Specificity of RNAi, LNA and CRISPRi as loss-of-function methods in transcriptional analysis. Nucleic Acids Res. 2018; 46 (12):5950–66. https://doi.org/10.1093/nar/gky437 PMID: 29860520

34. Chen S, Wang R, Zheng D, Zhang H, Chang X, Wang K, et al. The mRNA Export Receptor NXF1 Coordinates Transcriptional Dynamics, Alternative Polyadenylation, and mRNA Export. Mol Cell. 2019; 74 (1):118–31.e7. https://doi.org/10.1016/j.molcel.2019.01.026 PMID: 30819645

35. Jones E, Hummerich H, Viré E, Uphill J, Dimitriadis A, Speedy H, et al. Identification of novel risk loci and causal insights for sporadic Creutzfeldt-Jakob disease: a genome-wide association study. Lancet Neurol. 2020; 19(10):840–8. https://doi.org/10.1016/S1474-4422(20)30273-8 PMID: 32949544

36. de Leeuw CA, Mooij JM, Heskes T, Posthuma D. MAGMA: generalized gene-set analysis of GWAS data. PLoS Comput Biol. 2015; 11(4):e1004219. https://doi.org/10.1371/journal.pcbi.1004219 PMID: 25885710

37. Mishra A, Macgregor S. VEGAS2: Software for More Flexible Gene-Based Testing. Twin Res Hum Genet. 2015; 18(1):86–91. https://doi.org/10.1017/thg.2014.79 PMID: 25518859

38. Chavez A, Scheiman J, Vora S, Pruitt BW, Tuttle M, P R Iyer E, et al. Highly efficient Cas9-mediated transcriptional programming. Nat Methods. 2015; 12(4):326–8. https://doi.org/10.1038/nmeth.3312 PMID: 25730490

39. Van Etten J, Schagat TL, Hrit J, Weidmann CA, Brumbaugh J, Coon JJ, et al. Human Pumilio proteins recruit multiple deadenylases to efficiently repress messenger RNAs. J Biol Chem. 2012; 287 (43):36370–83. https://doi.org/10.1074/jbc.M112.373522 PMID: 22955276

40. Bohn JA, Van Etten JL, Schagat TL, Bowman BM, McEachin RC, Freddolino PL, et al. Identification of diverse target RNAs that are functionally regulated by human Pumilio proteins. Nucleic Acids Res. 2018; 46(1):362–86. https://doi.org/10.1093/nar/gkx1120 PMID: 29165587

41. Muppirala UK, Honavar VG, Dobbs D. Predicting RNA-protein interactions using only sequence information. BMC Bioinformatics. 2011; 12:489. https://doi.org/10.1186/1471-2105-12-489 PMID: 22192482

42. Kedde M, van Kouwenhove M, Zwart W, Oude Vrielink JA, Elkon R, Agami R. A Pumilio-induced RNA structure switch in p27-3' UTR controls miR-221 and miR-222 accessibility. Nat Cell Biol. 2010; 12 (10):1014–20. https://doi.org/10.1038/ncb2105 PMID: 20818387

43. Dörrbaum AR, Kochen L, Langer JD, Schuman EM. Local and global influences on protein turnover in neurons and glia. Elife. 2018;7. https://doi.org/10.7554/eLife.34202 PMID: 29914620

44. Gilbert LA, Larson MH, Morsut L, Liu Z, Brar GA, Torres SE, et al. CRISPR-mediated modular RNA-guided regulation of transcription in eukaryotes. Cell. 2013; 154(2):442–51. https://doi.org/10.1016/j.cell.2013.06.044 PMID: 23849981

45. Kurata M, Wolf NK, Lahr WS, Weg MT, Kluesner MG, Lee S, et al. Highly multiplexed genome engineering using CRISPR/Cas9 gRNA arrays. PLoS One. 2018; 13(9):e0198714. https://doi.org/10.1371/journal.pone.0198714 PMID: 30222773

46. Boeva V, Louis-Brennetot C, Peltier A, Durand S, Pierre-Eugène C, Raynal V, et al. Heterogeneity of neuroblastoma cell identity defined by transcriptional circuitries. Nat Genet. 2017; 49(9):1408–13. https://doi.org/10.1038/ng.3921 PMID: 28740262

47. Bettayeb K, Chang JC, Luo W, Aryal S, Varotsis D, Randolph L, et al. δ-COP modulates Aβ peptide formation via retrograde trafficking of APP. Proc Natl Acad Sci U S A. 2016; 113(19):5412–7. https://doi.org/10.1073/pnas.1604156113 PMID: 27114525

48. Hirst J, Barlow LD, Francisco GC, Sahlender DA, Seaman MN, Dacks JB, et al. The fifth adaptor protein complex. PLoS Biol. 2011; 9(10):e1001170. https://doi.org/10.1371/journal.pbio.1001170 PMID: 22022230

49. Tamgüney G, Giles K, Glidden DV, Lessard P, Wille H, Tremblay P, et al. Genes contributing to prion pathogenesis. J Gen Virol. 2008; 89(Pt 7):1777–88. https://doi.org/10.1099/vir.0.2008/001255-0 PMID: 18559949

50. Peters HL, Yan Y, Solheim JC. APLP2 regulates the expression of MHC class I molecules on irradiated Ewing's sarcoma cells. Oncoimmunology. 2013; 2(10):e26293. https://doi.org/10.4161/onci.26293 PMID: 24353913

51. Roisman LC, Han S, Chuei MJ, Connor AR, Cappai R. The crystal structure of amyloid precursor-like protein 2 E2 domain completes the amyloid precursor protein family. FASEB J. 2019; 33(4):5076–81. https://doi.org/10.1096/fj.201802315R PMID: 30608876

52. Millhauser GL. Copper binding in the prion protein. Acc Chem Res. 2004; 37(2):79–85. https://doi.org/10.1021/ar0301678 PMID: 14967054

53. Hopkins PC, Sáinz-Fuertes R, Lovestone S. The impact of a novel apolipoprotein E and amyloid-β protein precursor-interacting protein on the production of amyloid-β. J Alzheimers Dis. 2011; 26(2):239–53. https://doi.org/10.3233/JAD-2011-102115 PMID: 21593558

54. Aguzzi A, Haass C. Games played by rogue proteins in prion disorders and Alzheimer's disease. Science. 2003; 302(5646):814–8. https://doi.org/10.1126/science.1087348 PMID: 14593165

55. Chen Y, Wang X. miRDB: an online database for prediction of functional microRNA targets. Nucleic Acids Res. 2020; 48(D1):D127–D31. https://doi.org/10.1093/nar/gkz757 PMID: 31504780

56. Andréasson C, Ott M, Büttner S. Mitochondria orchestrate proteostatic and metabolic stress responses. EMBO Rep. 2019; 20(10):e47865. https://doi.org/10.15252/embr.201947865 PMID: 31531937

57. Hsiao K, Baker HF, Crow TJ, Poulter M, Owen F, Terwilliger JD, et al. Linkage of a prion protein missense variant to Gerstmann-Sträussler syndrome. Nature. 1989; 338(6213):342–5. https://doi.org/10.1038/338342a0 PMID: 2564168

58. Büeler H, Aguzzi A, Sailer A, Greiner RA, Autenried P, Aguet M, et al. Mice devoid of PrP are resistant to scrapie. Cell. 1993; 73(7):1339–47. https://doi.org/10.1016/0092-8674(93)90360-3 PMID: 8100741

59. Douet JY, Lacroux C, Corbière F, Litaise C, Simmons H, Lugan S, et al. PrP expression level and sensitivity to prion infection. J Virol. 2014; 88(10):5870–2. https://doi.org/10.1128/JVI.00369-14 PMID: 24574409

60. Minikel EV, Zhao HT, Le J, O'Moore J, Pitstick R, Graffam S, et al. Prion protein lowering is a disease-modifying therapy across prion strains, disease stages, and endpoints. bioRxiv. 2020.

61. Raymond GJ, Zhao HT, Race B, Raymond LD, Williams K, Swayze EE, et al. Antisense oligonucleotides extend survival of prion-infected mice. JCI Insight. 2019; 5. https://doi.org/10.1172/jci.insight.131175 PMID: 31361599

62. Martini PGV, Guey LT. A New Era for Rare Genetic Diseases: Messenger RNA Therapy. Hum Gene Ther. 2019; 30(10):1180–9. https://doi.org/10.1089/hum.2019.090 PMID: 31179759

63. PubChem N. Ambion/Life Technologies whole genome siRNA sequence database 2013 [Available from: https://www.ncbi.nlm.nih.gov/pcsubstance?term=%2522Life%20Technologies,%20Applied%20Biosystems,%20Ambion%2522.

64. Polymenidou M, Moos R, Scott M, Sigurdson C, Shi YZ, Yajima B, et al. The POM monoclonals: a comprehensive set of antibodies to non-overlapping prion protein epitopes. PLoS One. 2008; 3(12):e3872. https://doi.org/10.1371/journal.pone.0003872 PMID: 19060956